Supplementary Materials

Probing Binding and Allosteric Mechanisms of the KRAS Interactions with Monobodies and Affimer Proteins : Ensemble-Based Mutational Profiling and Thermodynamic Analysis of Binding Energetics and Allostery Reveal Diversity of Functional Hotspots and Cryptic Pockets Linked by Conserved Communication Network

Mohammed Alshahrani,[1] Vedant Parikh,[1] Brandon Foley,[1] Guang Hu,[2,3] Gennady Verkhivker[1,4]*

[1]Keck Center for Science and Engineering, Schmid College of Science and Technology, Chapman University, Orange, CA 92866, United States of America; alshahrani@chapman.edu (M.A.); verkhivk@chapman.edu (G.V).

[2]Department of Bioinformatics and Computational Biology, School of Life Sciences, Suzhou Medical College of Soochow University, Suzhou, 215213, China; huguang@suda.edu.cn (G.H.)

[3]Jiangsu Province Engineering Research Center of Precision Diagnostics and Therapeutics Development, Soochow University, Suzhou 215123, China; huguang@suda.edu.cn (G.H.)

[4]Department of Biomedical and Pharmaceutical Sciences, Chapman University School of Pharmacy, Irvine, CA 92618, United States of America; verkhivk@chapman.edu (G.V.)

* Correspondence: verkhivk@chapman.edu (G.V)

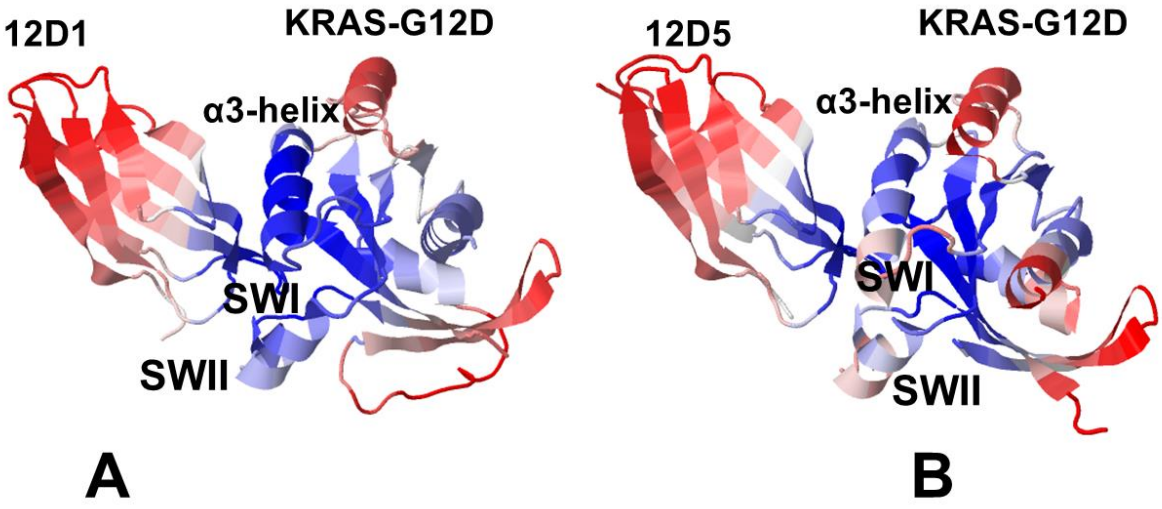

Figure S1. Structural maps of the essential mobility profiles for the KRAS-G1D complexes with monobody 12D1 (A) and monobody 12D5 (B). The essential mobility profiles are averaged over the first three major low frequency modes. The structures are shown in ribbons with the rigidity-to-flexibility scale colored from blue to red**.**

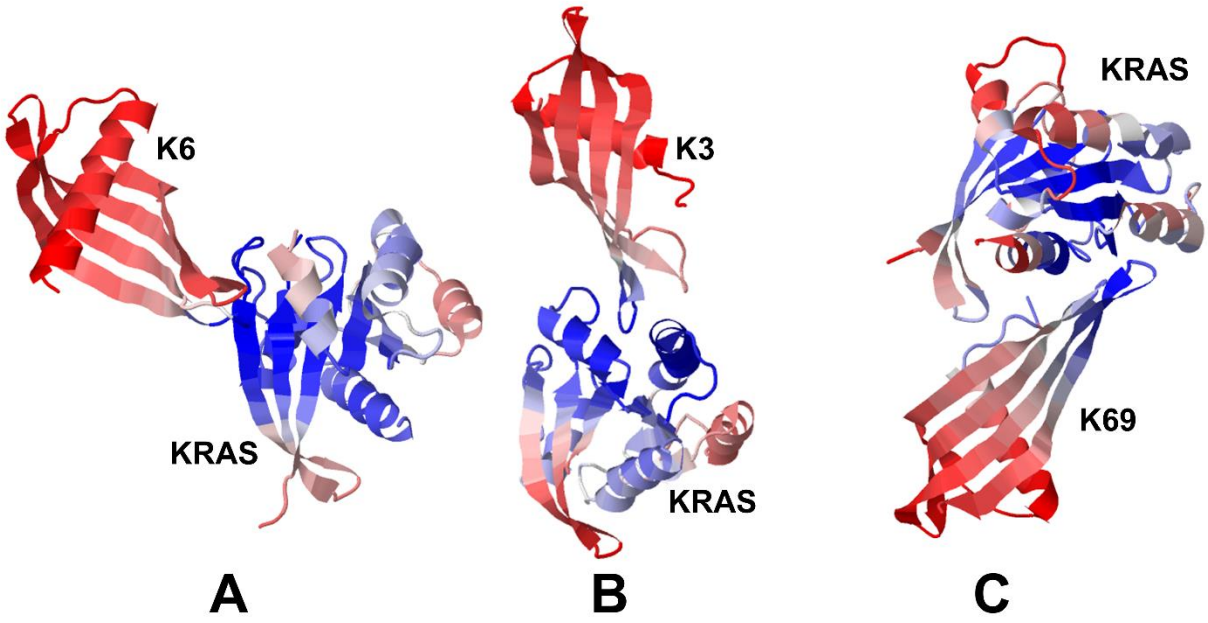

Figure S2. Structural maps of the essential mobility profiles for the KRAS-G1D complexes with affimer protein K6 (A), affimer protein K3 (B) and affimer protein K69 (C). The essential mobility profiles are averaged over the first three major low frequency modes. The structures are shown in ribbons with the rigidity-to-flexibility scale colored from blue to red**.**

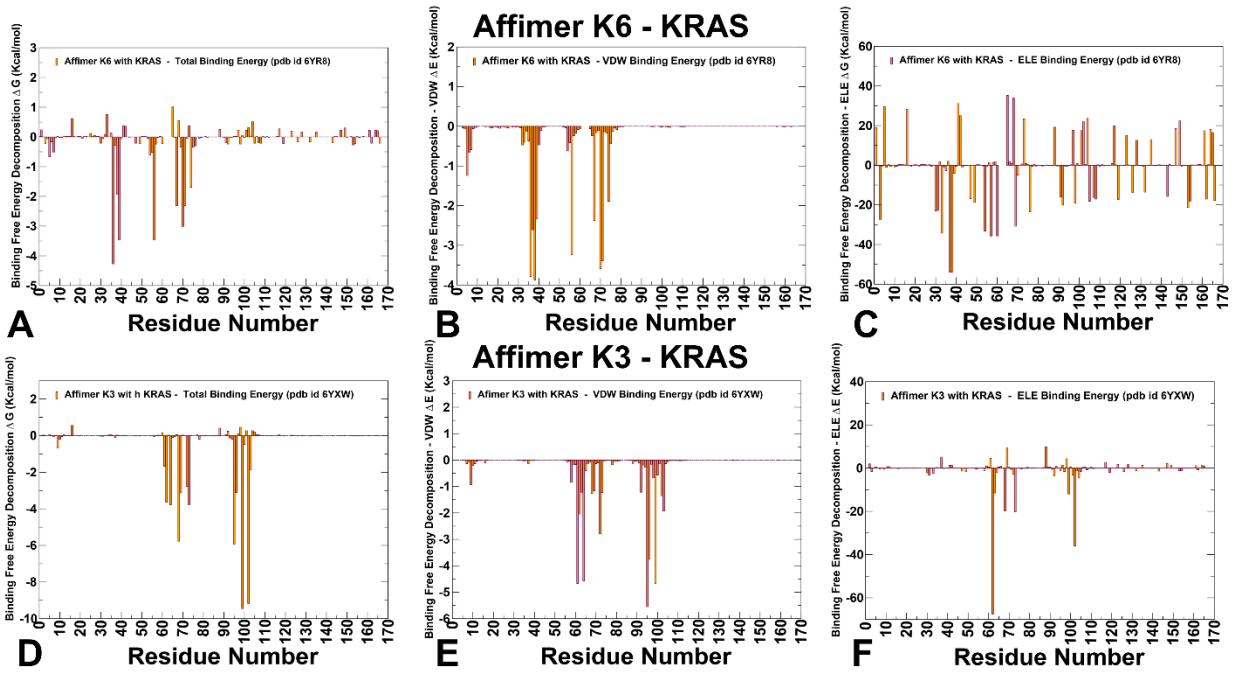

Figure S3. The residue-based decomposition of the total binding MM-GBSA energies for the KRAS residues in the KRAS complex with affimer K6 (A-C) and affimer K3 (D-F). The residue-based decomposition of the total binding energy (A), van der Waals contribution (B) and electrostatic contribution to the total MM-GBSA binding energy (C) for the KRAS residues in the KRAS complex with affimer K6 . The residue-based decomposition of the total binding energy (D), van der Waals contribution (E) and electrostatic contribution to the total MM-GBSA binding energy (F) for the KRAS residues in the KRAS complex with affimer K3. The MM-GBSA contributions are evaluated using 1,000 samples from the equilibrium MD simulations of respective KRAS complexes.

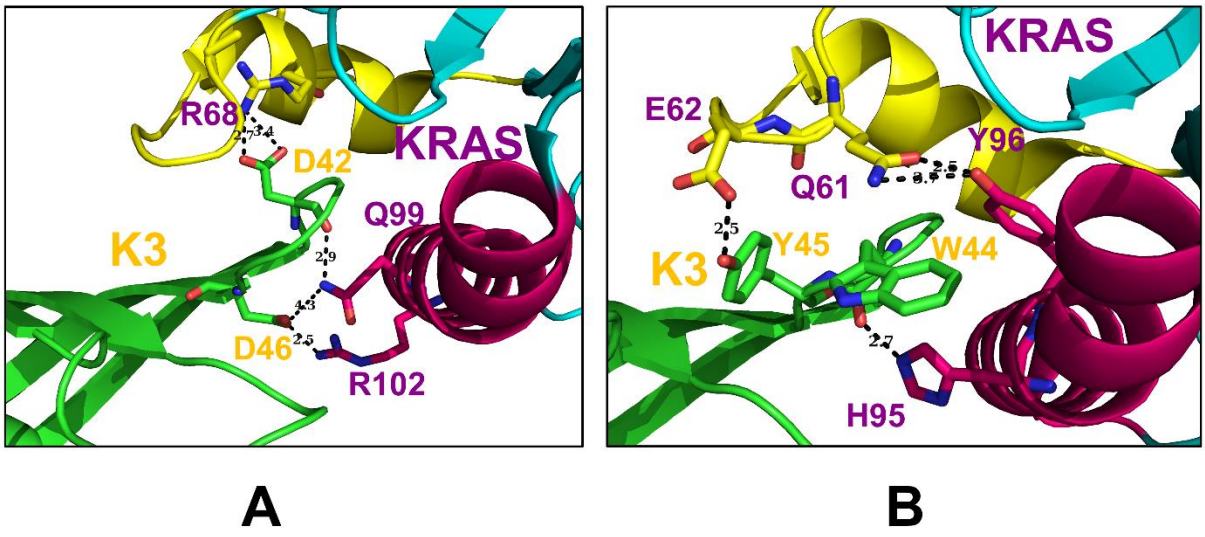

Figure S4. The interaction networks between KRAS and affimer K3 (A) Affimer K3 residues D42 and D46 (in orange) bind to R68 of SII α- 3 (dark purple) and Q99 and R102 of α-3 (dark purple) bringing the two α helices in proximity. (B) The intermolecular interactions formed by W44 side chain and Y45 (in orange) of K3 burying into hydrophobic pocket and forming hydrogen bond with H95 of α-helix 3 (in dark purple) and E62 of SII (in dark purple). When affimer K3 binds to the SII region, the D42 residue of K3 brings the SII region close to the α-3 helix by generating a hydrogen bond between R68 of SII and Q99 of α-3 helix. The complex formation is further strengthened by hydrogen bonds between side chain oxygen of D46 residue in K3 with the main chain nitrogens of Q99 and R102 in the α3-helix region of KRAS. This hydrogen bonding network anchors binding interfaces where I41, I43, W44 of K3 form hydrophobic interactions with V9, M72, V103, and H95 of KRAS.

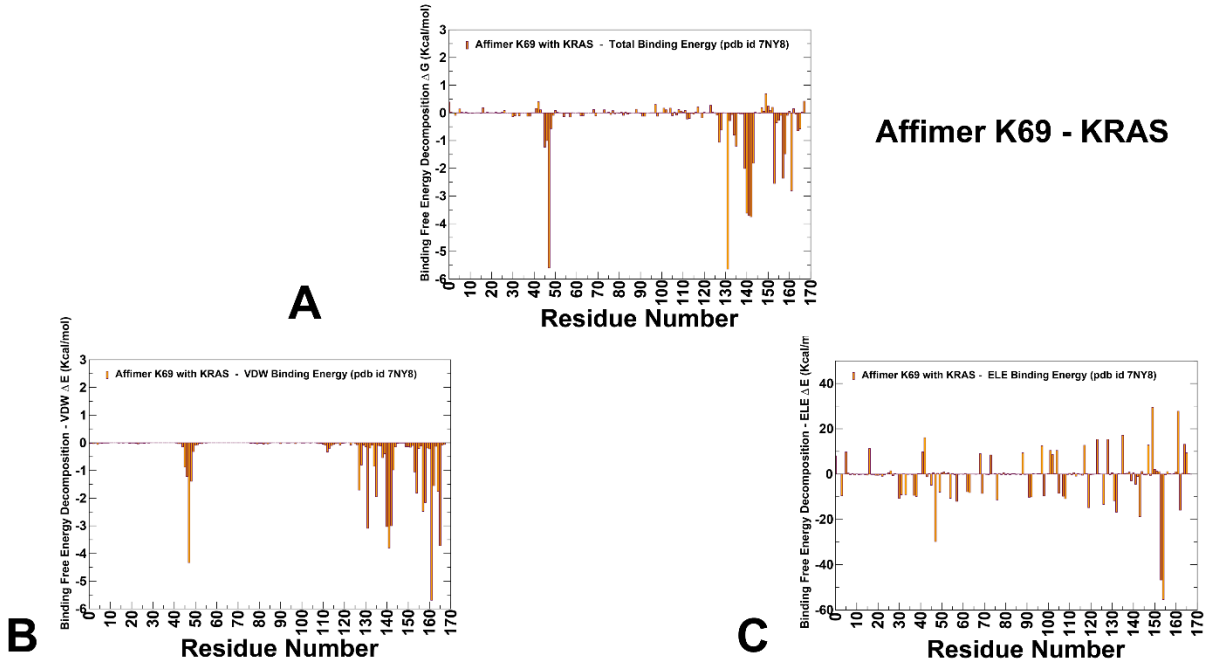

Figure S5. The residue-based decomposition of the total binding MM-GBSA energies for the KRAS residues in the KRAS complex with affimer K69. The residue-based decomposition of the total binding energy (A), van der Waals contribution (B) and electrostatic contribution to the total The MM-GBSA contributions are evaluated using 1,000 samples from the equilibrium MD simulations of KRAS-K69 complex.

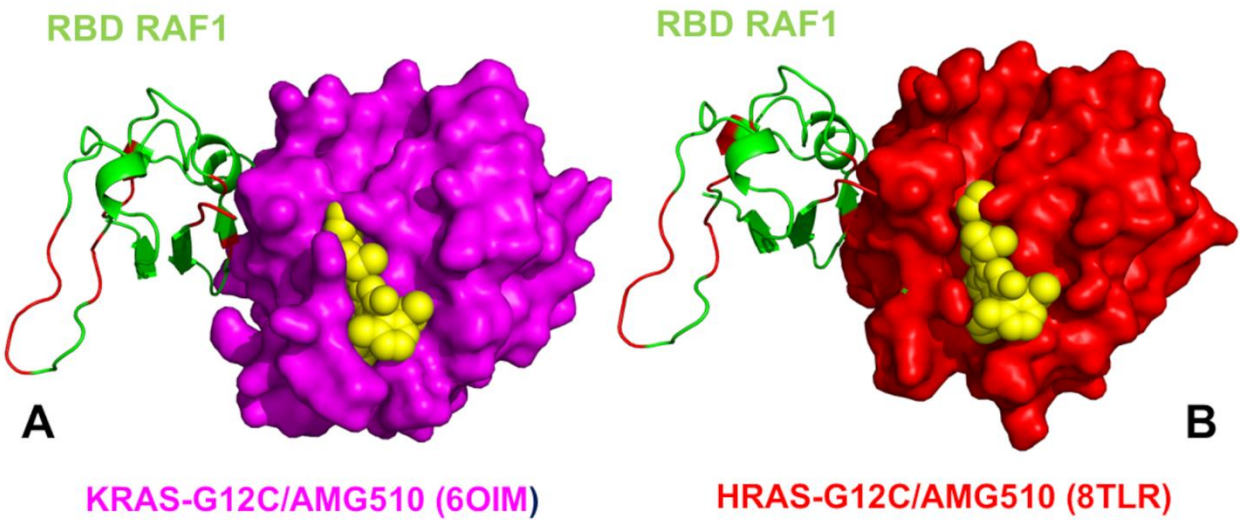

Figure S6. (A) The crystal structure of the human KRAS-G12C complex with RAF1 and allosteric inhibitor AMG510 KRAS-G12C is in magenta surface. RBD RAF1 is in green ribbons. AMG510 is in yellow spheres. The crystal structure of the human KRAS-G12C complex with RAF1 and allosteric inhibitor AMG510. (B) The crystal structure of the HRAS-G12C complex with RAF1 and allosteric inhibitor AMG510. HRAS-G12C complex (red surface), RBD RAF1 is in green ribbons and bound allosteric inhibitor AMG510 is yellow spheres.